Near-real time cloud properties and aircraft icing indices from GEO and LEO satellites

Patrick Minnis*[a], William L. Smith, Jr.[a], Louis Nguyen[a], D. A. Spangenberg[b], Patrick W. Heck[c]
Rabindra Palikonda[b], J. Kirk Ayers[b], Cory Wolff[d], John J. Murray[a]

[a]Atmospheric Sciences, MS 420, NASA Langley Research Center, Hampton, VA USA 23681
[b]AS&M, Inc., 1 Enterprise Parkway, Suite 300, Hampton, VA USA 23666
[c]CIMSS, University of Wisconsin-Madison, 1225 W. Dayton St., Madison, WI USA 53706
[d]National Center for Atmospheric Research, 3450 Mitchell Ln., Boulder, CO USA 80301

Earth Observing Systems IX Conference
International Symposium on Optical Science and Technology
SPIE 49th Annual Meeting
Denver, CO
2-6 August 2004

Near-real time cloud properties and aircraft icing indices from GEO and LEO satellites

Patrick Minnis*[a], William L. Smith, Jr.[a], Louis Nguyen[a], D. A. Spangenberg[b], Patrick W. Heck[c]
Rabindra Palikonda[b], J. Kirk Ayers[b], Cory Wolff[d], John J. Murray[a]

[a]Atmospheric Sciences, MS 420, NASA Langley Research Center, Hampton, VA USA 23681
[b]AS&M, Inc., 1 Enterprise Parkway, Suite 300, Hampton, VA USA 23666
[c]CIMSS, University of Wisconsin-Madison, 1225 W. Dayton St., Madison, WI USA 53706
[d]National Center for Atmospheric Research, 3450 Mitchell Ln., Boulder, CO USA 80301

ABSTRACT

Imagers on many of the current and future operational meteorological satellites in geostationary Earth orbit (GEO) and lower Earth orbit (LEO) have enough spectral channels to derive cloud microphysical properties useful for a variety of applications. The products include cloud amount, phase, optical depth, temperature, height and pressure, thickness, effective particle size, and ice or liquid water path, shortwave albedo, and outgoing longwave radiation for each imager pixel. Because aircraft icing depends on cloud temperature, droplet size, and liquid water content as well as aircraft variables, it is possible to estimate the potential icing conditions from the cloud phase, temperature, effective droplet size, and liquid water path. A prototype icing index is currently being derived over the contiguous USA in near-real time from Geostationary Operational Environmental Satellite (GOES-10 and 12) data on a half-hourly basis and from NOAA-16 Advanced Very High Resolution (AVHRR) data when available. Because the threshold-based algorithm is sensitive to small errors and differences in satellite imager and icing is complex process, a new probability based icing diagnosis technique is developed from a limited set of pilot reports. The algorithm produces reasonable patterns of icing probability and intensities when compared with independent model and pilot report data. Methods are discussed for improving the technique for incorporation into operational icing products.

keywords: aircraft icing, clouds, remote sensing, cloud microphysics, GOES, MODIS, AVHRR, air safety

1. INTRODUCTION

With the advent of multispectral imagers on GEO and LEO satellites, it is possible to derive a variety of valuable cloud and radiative properties in near-real time for many different applications. Data from GOES have been analyzed to produce such parameters on a near-real time basis[1] since 2000 over a limited domain in the central United States (US) centered on the Atmospheric Radiation Measurement[2] (ARM) Southern Great Plains site. During the daytime, the analyses produce reasonably accurate cloud effective particle sizes, optical depths, and water paths.[3,4,5] The results have been used for developing a cloud climatology for the area and for modeling studies of cloud and radiative processes. The near-real time products are also being generated from GOES-9 data over the ARM tropical western Pacific sites and evnvirons.[6] Data from the Visible infrared Scanner on the Tropical Rainfall Measuring Mission satellite and the Moderate Resolution Imaging Spectroradiometer (MODIS) on Terra and Aqua have been analyzed globally post facto since the launch of each satellite for better understanding of the radiation budget as part of the Clouds and Earth's Radiant Energy System (CERES).[7] GOES-8 data were analyzed in near-real time over Florida during the July 2002 CRYSTAL-FACE[8] (Cirrus Regional Study of Tropical Anvils and Cirrus Layers, Florida Area Cirrus Experiment) and over the northeastern US and southeastern Canada during the Atlantic THORpex Regional Campaign (AtReC) and Alliance Research Study II (AIRS2-II), respectively, conducted during late 2003. The results were used for mission

* p.minnis@nasa.gov; phone 1 757 864-5671; fax 1 757 864-7996; www-pm.larc.nasa.gov

planning, in-flight aircraft guidance, and rapid post mission analyses and debriefings. By comparing the results with in situ liquid water content (LWC), droplet size, and icing measurements, it was evident that these products are useful for diagnosing aircraft icing conditions as well as for validation of and assimilation into numerical models.

Because aircraft icing is one of the most dangerous weather conditions for general aviation, it is highly desirable to accurately determine, first, where icing conditions are present and will likely occur in both vertical and horizontal coordinates and, second, disseminate that information to pilots so that they can take the proper actions to avoid or accommodate those conditions. A Current Icing Potential (CIP) product was developed to combine model forecasts, surface observations, and pilot reports (PIREPS) assess the icing conditions in a particular area within the US.[9,10] Such data are often uncertain or sparsely available. Improvements in the temporal and areal coverage of icing diagnoses and prognoses would mark a substantial enhancement of aircraft safety in regions susceptible to heavy supercooled liquid water clouds. The use of 3.9-µm data from meteorological satellite imagers for diagnosing icing conditions has long been recognized[11] but to date, no explicit physically based methods have been implemented. Recent advances in cloud detection and cloud property retrievals using operational satellite imagery open the door for real-time objective applications of those satellite datasets for a variety of weather phenomena. Because aircraft icing is related to cloud macro- and microphysical properties,[12] it is obvious that cloud properties derived from satellite data should be useful for diagnosing icing conditions. To enhance the CIP, the NASA Advanced Satellite Aviation-weather Products (ASAP) project began sponsoring the development of near-real time retrievals of cloud products over the continental US (CONUS). This paper documents the current state of the CONUS cloud products and presents a prototype icing product that can be derived from both GEO and LEO data.

2. DATA & METHODOLOGY

The datasets used in the retrievals in this study include half-hourly GOES-8, 10, and 12 4-km spectral radiances. The GOES-8 and 10 imagers measure radiances at 0.65, 3.9, 10.8, and 12 µm. A 13.3-µm channel replaces the 12-µm channel on GOES-12 which took over for GOES-8 at 75°W in April 2002, while GOES-10 remains at 135°W. Hourly Rapid Update Cycle (RUC) analyses[13] provide hourly profiles of temperature and humidity at spatial resolutions of 40 and 20 km before and after April 2002, respectively. The profiles are used to assign height from the retrieved cloud temperature *Tc* and correct radiances for atmospheric attenuation. Clear-sky visible (VIS; 0.65 µm) reflectance for each location is derived from the 10' clear-sky albedo map used by the CERES project.[14] Spectral surface emissivity derived from GOES[15] and CERES[16] data are used with the RUC data to specify clear-sky radiating temperatures at 3.9, 10.8, and 12-µm. The data are ingested and analyzed within ~20 minutes of each GOES image. Pixels are classified as clear or cloudy based on a set of decision trees using all four channels.[17]

For clear pixels, the algorithm estimates the surface skin temperature and the outgoing longwave radiation (OLR), as well as the clear-sky VIS and shortwave (ASW) albedos, when appropriate. During daytime, when the solar zenith angle *SZA* is less than 82°, cloudy pixels are analyzed with the visible infrared solar-infrared split-window technique[1,18] (VISST). It matches the observed values with theoretical models of cloud reflectance and emittance.[19] At night, the solar-infrared infrared split-window technique (SIST) is used to retrieve all of the cloud properties. The SIST, an improved version of the 3-channel nighttime method,[18] uses thermal infrared data only. For each pixel, the methods retrieve effective cloud temperature *Tc*, cloud height *z* and thickness *h*, phase, optical depth *OD*, effective droplet radius *re* or effective ice crystal diameter *De*, and LWP or ice water path *IWP*. Supercooled liquid (SLW) clouds are those pixels with $Tc < 273$ K and a phase of liquid water. Other properties related to icing include *h*, *OD*, and *LWP*. The thickness is estimated using an empirical parameterization based on ARM cloud radar and satellite data.[20] Recently, a new method was introduced to derive low-level cloud heights because of the difficulty in accurately representing boundary-layer inversions in numerical weather analyses. The new method uses a fixed lapse rate anchored to the 24-hr running average surface temperature from the numerical weather model analysis. This new approach should minimize the cloud-top altitude overestimate that is common for low-level stratus clouds.

Many factors determine aircraft icing potential, but it generally requires supercooled liquid water, relatively large droplets, and large concentrations of droplets or high liquid water content (LWC). SLW can be discriminated from warm clouds using *Tc* and the concentration of large droplets should be related to *re*. LWC can be estimated as LWP/*h*. However, since both LWP and *h* depend on *t*, only LWP is used here as a proxy for LWC. Some weak positive depen-

Table 1. Strawman satellite-based icing intensity algorithm[25].

Icing Index	Classification Criteria			Icing Potential
0	clear, $Tc > 272$ K, $LWP < 100$ gm^{-2}, or ice cloud with $OD < 8$			none
1	ice cloud with $OD > 8$			unknown, indeterminate
	re (μm)	LWP (gm^{-2})	Tc (K)	
2	> 11	> 100	< 272	low
3	> 11	> 200	< 272	medium
4	> 11	> 300	<272	high
5	> 9	> 400	<272	low
6	> 9	> 500	< 272	medium
7	> 11	> 300	<253	high
8	>9	> 400	< 253	high

dencies of icing intensity on LWP and *re*, and a weak negative dependency on *Tc* were found using matched VISST and in situ aircraft data.[22,23,24]

Using those results as guidelines, a strawman icing classification system[25] was initiated to begin development of a reliable algorithm for converting real-time cloud properties to icing assessments. Table 1 summarizes this prototype algorithm. It is assumed that the icing index (II) is 0 or no icing is likely when no clouds are present, no SLW is detectable, the cloud is relatively thin (LWP < 100 g m^{-2}), the retrieved cloud is classified as optically thin ice, or the results do not satisfy any of the other criteria. If the cloud is determined to be optically thick and composed of ice, then it is assumed that the icing conditions are indeterminate (II=2) because the upper ice cloud may or may not hide a lower-level SLW cloud. The remaining classifications are various icing categories of low, medium, or high icing potential that depend on *re*, *LWP*, and *Tc*. The criteria are based on the assumption that icing potential increases with increasing *re* and *LWP*, and decreasing *Tc*. These classes will be used until enough statistical data from PIREPS and field programs can be gathered to verify or to alter this classification system.

The cloud property and icing methodology is currently being applied in near-real time to GOES-10 data between 25°N and 50°N and 100°W and 130°W and to GOES-12 data between 25°N and 50°N from 65°W to 100°W. The results are derived separately and stitched together to form a CONUS dataset that is available on the World Wide Web (http://www-angler.larc.nasa.gov/satimage/products.html) in image or digital formats. Given the horizontal locations, the vertical location of the potential icing clouds can be estimated from the cloud-top and base altitudes of the clouds.

3. RESULTS

Figure 1 shows an example of the CONUS results for GOES-10/12 imagery taken at 1545 UTC, 15 March 2004. The pseudocolor RGB image (Figure 1a) is used to reveal the various cloud types in a single image. In this type of image, red is assigned to the visible reflectance, the temperature difference between the 3.9 and 11-μm channels determines the green intensity, and the 11-μm temperature *T* provides the blue intensity on an inverse scale. Snow-free clear areas like much of the western CONUS and northern Mexico are green, blue, or tan while clear snow-covered areas such as western Wyoming and south central Canada are typically bright or dark pink. High clouds are generally white (e.g, Gulf of Mexico), grey (e.g., northern Ohio), or some shade of magenta (e.g., South Dakota to Wisconsin), while low or midlevel clouds are often white (e.g., New York) or a shade of peach or orange (e.g., Texas and Arkansas). The retrieved cloud phase image shows clear areas in green, warm liquid water clouds in dark blue, SLW clouds in light blue, and ice clouds in red. Some of the scattered dark blue clouds over the western US are actually misclassified clear areas because the clear-sky albedo map has not yet been optimized for the GOES VIS spectral band. The derived values of *re* (Figure 1c) are typically between 7 and 11 μm but can be smaller (e.g., southwest corner of image) or greater (e.g., off southern

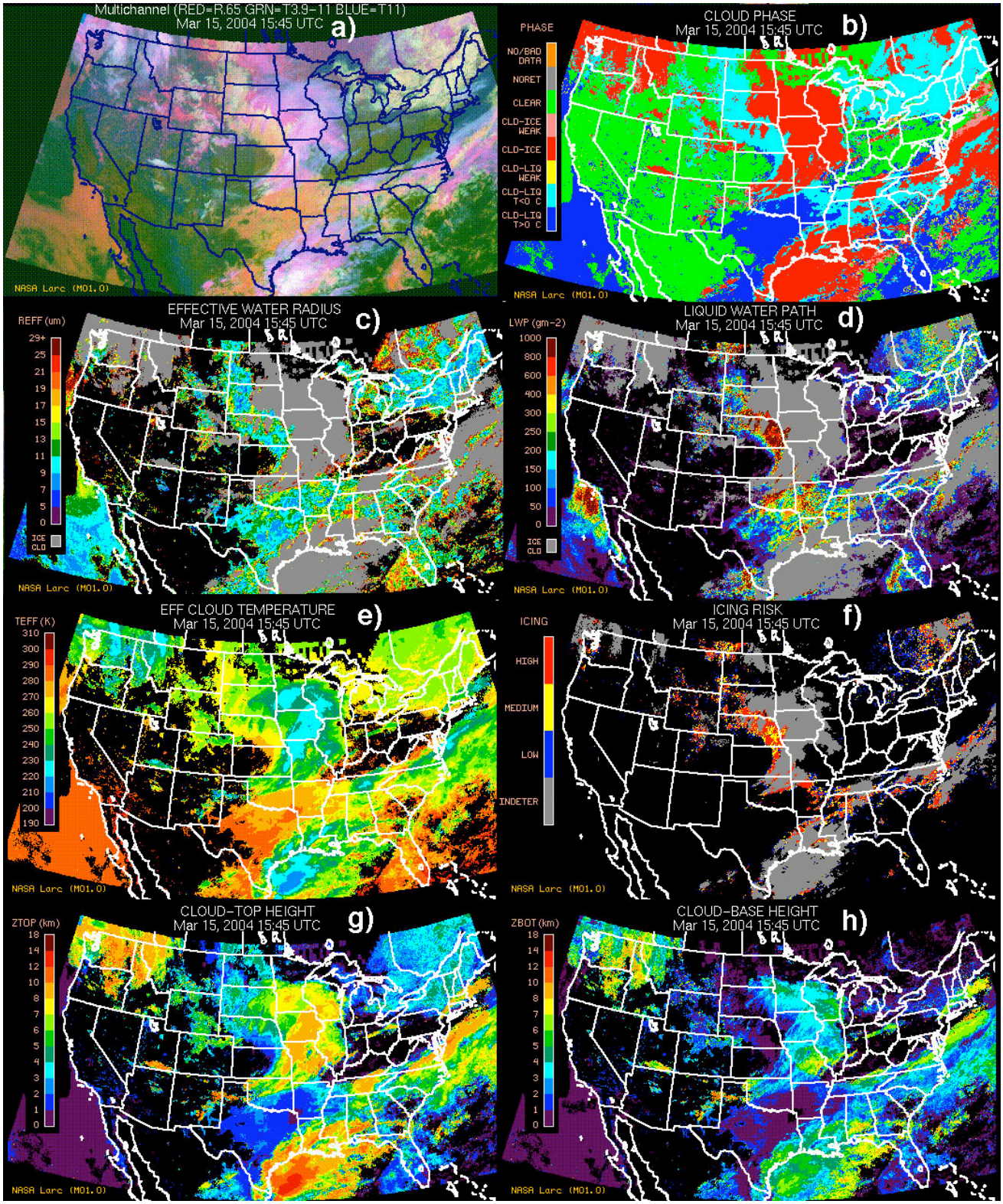

Figure 1: Merged GOES-10 and 12 (a) pseudocolor images and (b-h) cloud and icing parameters 1545 UTC, 15 March 2004.

California coast). In some overlapped conditions along the edges of ice clouds (e.g., central Oklahoma) or for relatively thin clouds over snow (southeastern Canada), the VISST will retrieve a large value of *re* because of contamination of the 3.9-μm radiance by ice in form of large cirrus crystals or snow grains. The cloud LWP reaches extremely high values, exceeding 500 gm^{-2}, off the California coast and over eastern Nebraska. More often, *LWP* is less than 200 gm^{-2} in this image (Figure 1d). The effective cloud temperatures (Figure 1e) for most of the liquid-water clouds in the southern half of the image are greater than 270 K. The value of *Tc* for most of the SLW clouds is greater than 253 K.

The data in Figures 1b-e and the criteria in Table 1 were used to produce the icing risk or potential map in Figure 1f. The greatest potential is diagnosed over Nebraska, northern Colorado, and southern Canada. The other areas of high risk include Oklahoma, Arkansas, and Mississippi and other locations. The high-risk classification in some of those cases might result from the large value of *re* that occurred as a result of the cirrus overlap. Exactly which pixels were affected requires further analysis. Not all of the SLW clouds over southeastern Canada are classified as being an icing risk. The cloud deck is inhomogeneous so that the pixels diagnosed to contain icing conditions are scattered in space and in intensity. Many of the clouds have values of $re < 9$ μm, a condition that would rule them out according to the strawman algorithm. Cirrus clouds over Arizona and New Mexico and half of those in Minnesota and Wisconsin are ignored and given the no-icing classification because they are relatively thin. Most of the remaining ice-cloud pixels yield an indeterminate category because they are optically thick. The spurious low clouds over the western US noted above are always too thin and often too warm to result in a positive icing potential classification. Thus, they are not likely to induce in any errors in assessing icing risk, although they would be a nuisance in any cloud modeling validation or assimilation study. The vertical boundaries of the clouds posing a potential icing risk can be assessed from the cloud-top (Figure 1g) and base (Figure 1h) heights. Over eastern Nebraska, aircraft icing appears to be a threat between the surface and 5 km, over the central and northwestern CONUS are classified as indeterminate or unknown because they are optically thick.

The VISST products were generated throughout the AIRS-II and ATReC experiments during November and December 2003 using GOES-12, NOAA-16 AVHRR and *Terra* and *Aqua* MODIS data to provide a variety of views and resolutions to better understand the retrievals, provide support for the experiments, and validate the remote sensing methodologies. The various datasets are unprecedented for studying icing conditions. Figure 2 shows examples of the icing intensities determined over the domain from the three LEO satellites at nearly the same times as from the GOES-12 imager. The patterns of areas with icing potential in the first pair of images, taken ~9 min apart, are very similar except for more icing-free areas around 57°N, 72°W in the AVHRR results than retrieved from GOES-12. Both analyses yielded similarly large *OD*s, but they differed in the values of *re*. The AVHRR retrievals yielded effective droplet sizes as small as 5 μm in some areas while the least values from GOES-12 are 8 μm in the space between the two large areas with icing potential. Except for Nova Scotia, the actual intensities are very similar for the two retrievals. A retrieval using *Terra* MODIS data taken earlier in the same day (not shown) also produced patterns very similar to those from GOES-12, but the intensities were generally lower than the GEO values because of smaller optical depths. Icing intensities derived from *Aqua* MODIS and GOES-12 (not shown) are very similar in location and intensity.

4. DISCUSSION

An operational system that includes satellite retrievals over large areas such as Alaska and central Canada will necessarily include both LEO and GEO satellite data. The GEO satellites are best suited to covering the tropics and lower mid-latitudes while the LEO data will be used more often for areas poleward of 50° where the viewing zenith angle (VZA) can be quite large. For example, at 105°W, the VZA at 50°N is 62° rising to 72° at 60°N. Figure 2 illustrates that consistent results can be derived from different satellites viewing from completely different angles. For example, *Aqua* MODIS scans Maine at a VZA of ~21° in Figure 2c, while GOES-12 has a VZA of ~52°. The NOAA-16 and GOES-12 VZA's in Figures 2a and b differ by ~13°. Inter-satellite consistency is important because it indicates that few algorithmic changes will be needed when switching data sources from one satellite to another. However, the differences hint at a potential problem with using the threshold approach. Small changes in *re* or *LWP* can cause a potentially dangerous cloud to become classified as a no-icing case. Given the uncertainties in the retrievals, such small misclassifications could be frequent.

The results presented above serve as samples of the products currently being generated, but, as noted earlier, the algorithm for icing intensity is still in the formulation stage. In situ data from a variety of field measurements as well as PIREPS have been used to relate cloud properties like those in Figure 1 to measurements of icing. [22,23,24] For example, it

has been shown that when overlying cirrus clouds were absent, the VISST retrieved SLW in 98% of the PIREPS reports of positive icing[22] indicating that the satellite can provide the first condition necessary to identify icing conditions. Determining the other conditions becomes more difficult. Thus, validation and improvement of the prototype algorithm has begun by comparing the in situ data from AtREC and other field programs.[25] However, developing clear-cut icing/no-icing thresholds is not likely to be possible because of the many different factors, like aircraft size, speed and residence time in the cloud, that determine icing besides the properties of the clouds themselves. Development of probabilities for icing conditions based on satellite data, similar to those used for the CIP, might be the best approach to convolving satellite products into the CIP.

For example, Figure 3 shows the merged GOES-10/12 RGB image (Figure 3a), the VISST-derived icing intensities (Figure 3b), and the total column experimental CIP for the CONUS around 1900 UTC for 18 March 2004 (Figure 3c) which includes some satellite information. When not indeterminate, the icing intensities from GOES generally coincide with the high-probability areas. Some exceptions include eastern Iowa, western South Dakota, over the Atlantic, and eastern Washington. In some of those areas, the PIREPS denote icing conditions. Although the algorithm identifies SLW clouds in those same areas, it does not classify them as conducive to icing because of the arbitrary thresholds used in the strawman algorithm.

In situ measurements can provide better understanding of the conditions causing icing and can validate the satellite-derived microphysical properties of the clouds, but the development of robust probability statistics will require thousands of comparisons with PIREPS over a wide range of cloud conditions over various landforms in different climates and seasons. To begin that process, data from the CONUS retrievals between October 2003 and March 2004, the heaviest icing season, are being compared with the PIREPS taken at 1545 and 2045 UTC. The comparisons use the average properties of the GOES pixel closest to the location of the PIREPS and the its four nearest neighbors. Although this matching is not perfect, it can account for some of the errors due to time differences between the satellite image and the report and between the occurrence of icing and the actual reporting and to spatial differences between the location of the aircraft icing and the location when it was reported.

At the time of this writing, only data taken over the eastern CONUS between 1 and 11 February 2004 have been analyzed yielding 2853 matched data points. Of those, both the algorithm in Table 1 and the PIREPS icing and no-icing conditions 8.6 and 27.3% of the time, respectively. The VISST analysis gave an indeterminate value for 33.6% of cases. Of those, the PIREPS reported icing conditions 75% of the time. For 26.7% of the PIREPS, the algorithm returned no icing when icing was reported by the pilots. In the remaining 3.9% of the PIREPS, no icing was recorded, but the VISST diagnosed icing conditions. These comparisons are somewhat consistent with the cursory analysis of Figure 3 and highlight the tendency of the thresholds to exclude many icing conditions. For the matched PIREPS and GOES icing diagnoses, the middle altitude of the icing layer was within the VISST-derived cloud top and base heights 55% of the time. The middle icing altitude was above the VISST cloud top in 40% of the cases and below the satellite cloud-base height in the remaining 5% of the matches. The error relative to cloud top is probably due to the errors in the method used to convert *Tc* to *Ztop*.

To develop a more probabilistic algorithm form the satellite data, histograms of no icing, light icing and moderate-to-severe (mod-sev) were developed as functions of cloud LWP, re, and Tc. The resulting normalized probabilities for a given icing category at a particular LWP are plotted in Figure 4a. In 40% of the cases when LWP < 100%, the PIREPS indicate that icing occurred regardless of *re*. Table 1 does not diagnose icing in any case when LWP < 100 gm^{-2}, thus explaining the underestimate in the comparisons. Only a weak dependence on re was found. The mean value for all mod-sev PIREPS is 12.6 μm compared to 11.1 and 10.9 μm for no-icing and light icing, respectively. On average, the icing clouds are 6-K colder than the no-icing clouds suggesting a dependence on *Tc*. However, the total amount of water in the cloud is the most reliable indicator of icing probability with average *LWP*'s of 266, 393, and 487 gm^{-2} for the no, light, and mod-sev icing categories. If the original 9 icing categories are considered, mean *LWP* increases monotonically with icing severity from 266 gm^{-2} for no icing up to 589 gm^{-2} for severe icing. Thus, as a first approximation icing probability from the VISST products will be determined as a function of *LWP* and *re*.

To improve the statistics, only two categories are considered for this initial icing probability model: no-icing and icing. The light and mod-sev probabilities in Figure 4a were combined and multiplied by the probabilities for icing at 5 and 16 μm. Those products were then normalized to the total conditional probabilities of icing and no icing for each *LWP* bin.

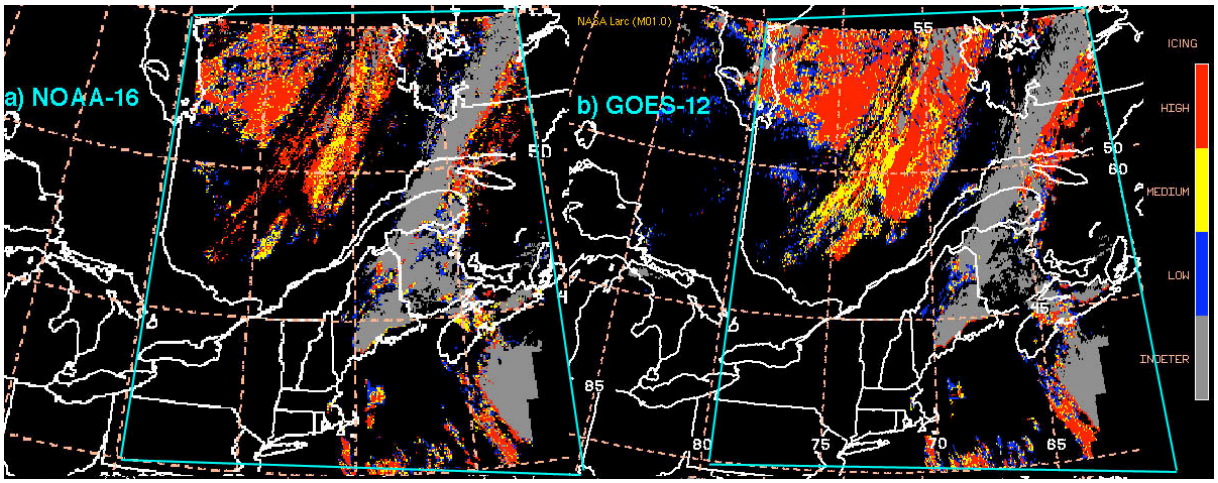

Figure 2: VISST-based icing intensities from matched satellites, 1745 UTC, 21 November 2003. Light blue boxes denote approximate boundaries of matched analysis areas for each pair of images.

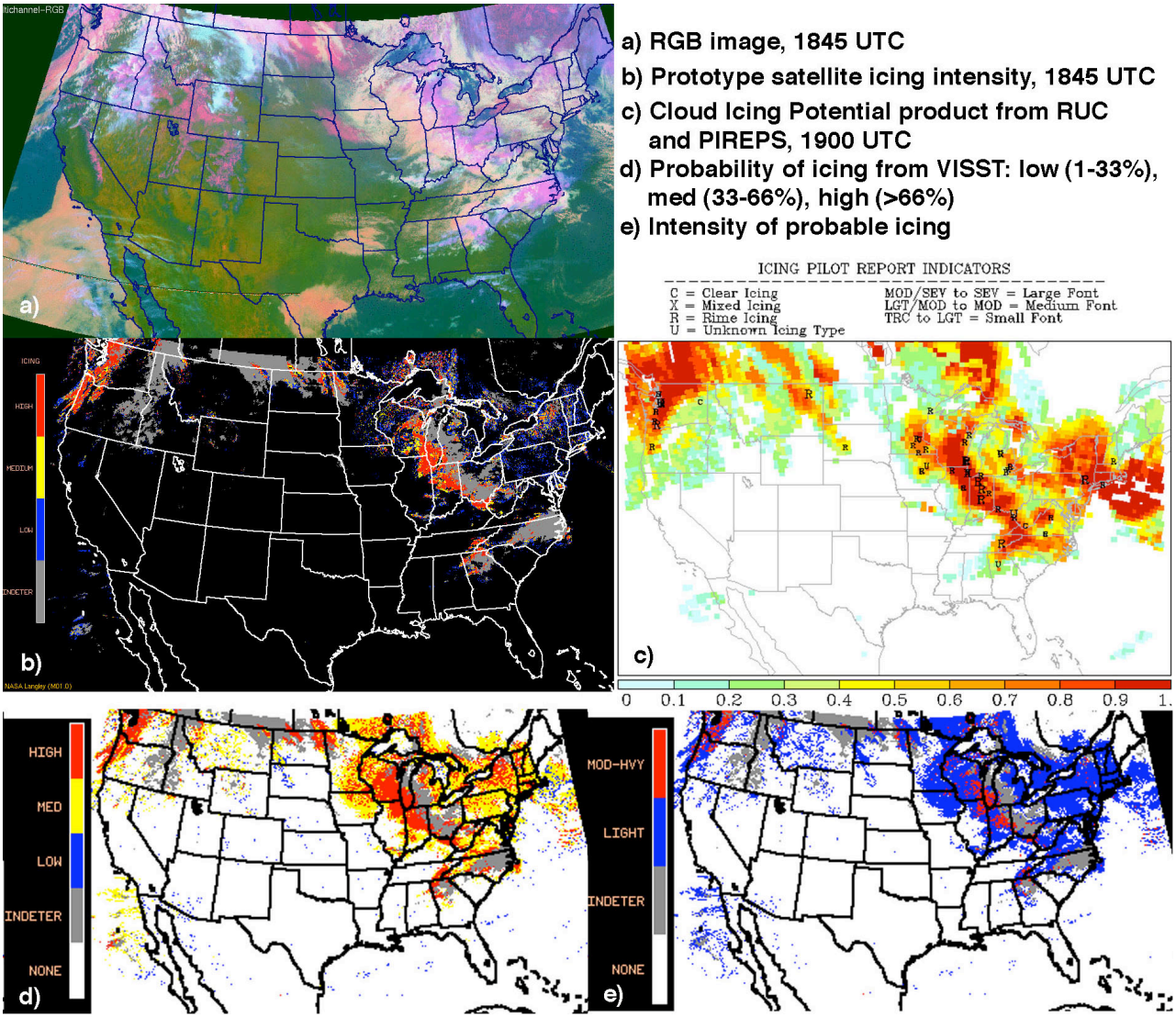

Figure 3: Comparison of GOES-estimated and experimental model-based icing potentials.

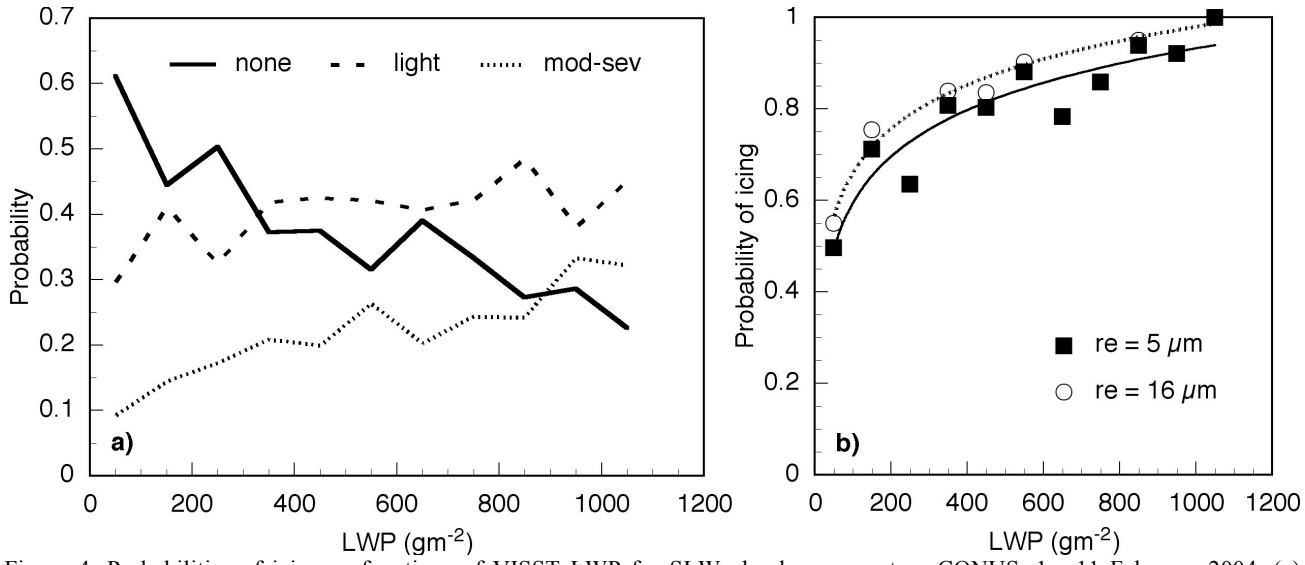

Figure 4: Probabilities of icing as functions of VISST LWP for SLW clouds over eastern CONUS, 1 - 11 February 2004. (a) categories from PIREPS, (b) Renormalized probabilities for all positive icing PIREPS and model fit for two values of *re*.

The resulting values were then renormalized by the ratio of unity to the probability of icing for *re* = 16 μm at *LWP* =1050 gm^{-2}. This renormalization was performed using the assumption that for a cloud containing large SLW droplets and more than 1000 gm^{-2} of liquid water, the probability of icing should be 100%. The resulting data points and regression fits are shown in Figure 4b. The fit for *re* = 16 μm was smoothed by dropping out some of the lower values that corresponded to bins with poor sampling. The resulting curves, which are based on a logarithmic fit, are used in a simple manner to estimate the icing probability from the VISST data.

Except for a slight change in the *OD* threshold, the new probability algorithm uses the same tests as Table 1 to initially screen out warm clouds, thin cirrus, clear, and indeterminate areas. The three former classes are assigned icing probabilities of zero. The percentage of indeterminate areas should increase because the *OD* threshold has been dropped to 6. All remaining pixels are assumed to be filled with SLW clouds. The value of LWP for each remaining pixel is used to determine the probabilities of icing at 5 and 16 μm using the curves in Figure 4b. If $re \leq 5$ μm, then the former probability is assigned to the pixel, or if $re \geq 16$ μm, the pixel is given the probability for *re* = 16 μm. Otherwise, the probability is determined by linearly interpolating between the two curves using the VISST-derived value of *re*. All negative probabilities are set equal to zero, while all of those exceeding 1.0 are given the value of 1.0. For all non-zero probabilities, the intensity of icing is estimated using the mean *LWP*'s for the light and mod-sev categories. Instead of three icing categories, only the light and mod-sev classes are estimated for this initial test.

This simple algorithm was applied to the VISST results used to create the icing intensities in Figure 3b. The resulting VISST-based probabilities and corresponding intensities are plotted in Figures 3d and 3e, respectively. The areas of potential icing are dramatically increased compared to those in Figure 3b. The pattern of positive probabilities tend to look a lot more like those in the experimental CIP (Figure 3c), but the higher probabilities cover more area than those in the CIP. All of the positive PIREPS in Figure 3c correspond to non-zero icing probabilities in Figure 3d. Nearly all of the moderate-severe PIREPS (Figure 3c) correspond to the mod-sev category in Figure 3e. One exception is the PIREP over northeastern Pennsylvania, where *LWP* < 200 gm^{-2}, but *re* is very large. There are some scattered individual pixels with low icing probabilities. These generally correspond to the edges of thin cirrus clouds. Other spurious positive icing returns are found over the Pacific off of Baja. These are due to thin cirrus over the warm stratus deck. In this case, the clouds are classified as water because the water signal is strongest, but *Tc* < 272 K. There are some marked differences between the CIP and the VISST icing probability that suggest the VISST should provide some improvement to the CIP. For example, the low CIP probabilities in the vicinity of the Minnesota, North Dakota, and Canada borders belie the existence of a distinct thick cloud bank over snow that is classified as a high probability area (Figure 3d).

The great number of pixels with large icing probabilities in Figure 3d compared to the experimental CIP is probably due to the artificially high renormalized values of probability in Figure 4b. The initial algorithm was developed to

demonstrate the utility of the VISST data for estimating reasonable icing probabilities. Many refinements of the algorithm are possible including the use of more explicit use of other independent variables such as *Tc* and *re*. Such improvements, however, await the matching of many more PIREPS and VISST retrievals to achieve a reliable statistical database.

4. CONCLUDING REMARKS

A new prototype, physically based method for real-time estimation of the probability of icing conditions has been demonstrated using merged GOES-10 and 12 data over the continental United States and southern Canada. The use of icing probability with an associated intensity rating appears to be a more reliable approach to diagnosing icing because it is less susceptible to small retrieval errors and to arbitrary thresholds. Because icing depends on so many different variables, such as aircraft size or air speed, it is not possible to achieve 100% success with a threshold or any other type of approach.

Although the initial algorithm shows great promise, much additional research must be completed before it can serve as a reliable input for the operational CIP. Currently, it returns icing probabilities for the cloud layer estimated from VISST. While this layer includes the center of the icing layer in 55% of the cases, 40% of the time, the PIREP finds icing above the satellite-retrieved cloud top. The delineation of the icing layer in terms of its vertical boundaries will need to be improved using either the RUC or balloon soundings or ceilometer data to adjust the cloud base height, a change that would require adjustment of *Ztop*. Only daytime data have been considered so far. While there is some skill in discriminating between optically thin and thick clouds at night using the SIST, the utility of resulting products for icing classification has not yet been examined. Most of the indeterminate cases were found to be a combination of a high ice cloud over an icing cloud. Better detection of multilayered clouds using multispectral IR data[26] or matched microwave and VIS data[27] would help minimize the number of indeterminate cases. Other ways to minimize the indeterminate cases could include using the ceilometer data along with RUC soundings to locate a lower-level cloud deck or, in a more universal approach, using empirical relationships between clouds and the RUC profiles[28] to diagnose clouds under the satellite-observed cirrus clouds. Similar methods are already being used to develop the current CIP product and could be adapted to work in a conditional probability scenario with the satellite retrievals. False returns caused by thin cirrus clouds over warm, low cloud decks can also be minimized by using the multispectral IR methods to detect thin cirrus clouds. Such techniques typically rely on the availability of 12-µm data, which are currently not taken by GOES-12. Hopefully, future GOES imagers will replace the 13.3-µm channel on GOES-12 with the original 12-µm channel.

The satellite icing algorithms are just one part of a comprehensive aircraft icing program being developed by NASA, NOAA, and the FAA. Ultimately, the results will be combined with PIREPS, model forecasts, and other data to provide a near-real time optimized characterization of icing conditions for pilots and flight controllers.

ACKNOWLEDGMENTS

This research was funded by the NASA Earth Science Enterprise and the NASA Aviation Safety Program through the NASA Advanced Satellite Aviation-weather Products Initiative. Additional support was provided by the Environmental Sciences Division of U.S. Department of Energy Interagency Agreement DE-AI02-97ER62341 through the ARM Program.

REFERENCES

1. Minnis, P., W. L. Smith, Jr., D. F. Young, L. Nguyen, A. D. Rapp, P. W. Heck, S. Sun-Mack, Q. Trepte, and Y. Chen, A near-real time method for deriving cloud and radiation properties from satellites for weather and climate studies. *Proc. AMS 11th Conf. Satellite Meteorology and Oceanography*, Madison, WI, Oct. 15-18, 477-480, 2001.
2. Ackerman, T., and G. Stokes, The Atmospheric Radiation Measurement Program, *Physics Today,* 56**,** 38 – 45, 2003.
3. Young, D. F., P. Minnis, D. Baumgardner, and H. Gerber, 1998: Comparison of in situ and satellite-derived cloud properties during SUCCESS. *Geophys. Res. Lett.*, **25**, 1125-1128.
4. Dong, X., P. Minnis, G. G. Mace, W. L. Smith, Jr., M. Poellot, R. T. Marchand, and A. D. Rapp, 2002: Comparison of stratus cloud properties deduced from surface, GOES, and aircraft data during the March 2000 ARM Cloud IOP. *J. Atmos. Sci.*, **59**, 3256-3284.

5. Min, Q, P. Minnis, and M. M. Khaiyer, 2004: Comparison of cirrus optical depths from GOES-8 and surface measurements. *J. Geophys. Res*., **109**, 10.1029/2003JD004390.
6. Khaiyer, M. M., M. L. Nordeen, P. Minnis, W. L. Smith, Jr., D. R. Doelling, and V. Chakrapani, 2004: Validation of cloud properties derived from GOES-9 over the ARM TWP region. *Proc. 14th ARM Science Team Meeting*, Albuquerque, NM, March 22-26. (Available at http://www.arm.gov/publications/proceedings/conf14/extended_abs/khaiyer-mm.pdf)
7. Minnis, P., D. F. Young, S. Sun-Mack, P. W. Heck, D. R. Doelling, and Q. Z. Trepte, 2003: CERES cloud property retrievals from imagers on TRMM, Terra, and Aqua. *SPIE 10th Intl. Symp Remote Sens., Conf. Remote Sens. Clouds and Atmos.*, Barcelona, Spain, September 8-12, 37-48.
8. Jensen, E., D. Starr, and O. Toon, Mission investigates tropical clouds. *Eos*, **85**, 45-50, 2004.
9. McDonough, F. and B.C. Bernstein, Combining satellite, radar and surface observations with model data to create a better aircraft icing diagnosis. *Proc. 8th AMS Conf. Aviation, Range, and Aerospace Meteorol.*, Dallas, TX, 10-15 January, 467-471, 1999.
10. Bernstein, B.C., F. McDonough, M.K. Politovich and B.G. Brown, CIP: physically-based, integrated approach to the diagnosis of in-flight aircraft icing, Part I: Algorithm description. Submitted, *Weather and Forecasting*, 2004.
11. Ellrod, G. and J. P. Nelson, 1996: Remote Sensing of Aircraft Icing Regions Using GOES Multispectral Imager Data, *Proc. AMS 15th Conf. Weather Anal. & Forecasting*, 19-23 August, Norfolk, VA, 9-12.
12. Cober, S. G., G. A. Isaac, and J. W. Strapp, 1995: Aircraft icing measurements in east coast winter storms. *J. Appl. Meteor.*, **34**, 88-100.
13. Benjamin, S. G., D. Dévényi, S. S. Weygandt, K. J. Brundage, J. M. Brown, G. A. Grell, D. Kim, B. E. Schwartz, T. G. Smirnova, and T. L. Smith, and G. S. Manikin, 2004: An hourly assimilation-forecast cycle - the RUC. *Mon. Wea. Rev.*, **132**, 495-518.
14. Sun-Mack, S., Y. Chen, T. D. Murray, P. Minnis, and D. F. Young, Visible clear-sky and near-infrared surface albedos derived from VIRS for CERES. *Proc. AMS 10th Conf. Atmos. Rad.*, Madison, WI, June 28–July 2, 422-425, 1999.
15. Smith, W. L., Jr., P. Minnis, D. F. Young, and Y. Chen, Satellite-derived surface emissivity for ARM and CERES. *Proc. AMS 10th Conf. Atmos. Rad.*, Madison, WI, June 28 – July 2, 410-413, 1999.
16. Chen, Y., S. Sun-Mack, Surface spectral emissivity derived from MODIS data. *Proc. SPIE Conf. Optical Remote Sens. of Atmosphere and Clouds III*, Hangzhou, China, Oct. 23-27, 361-369, 2002.
17. Trepte, Q., Y. Chen, S. Sun-Mack, P. Minnis, D. F. Young, B. A. Baum, and P. W. Heck, Scene identification for the CERES cloud analysis subsystem. *Proc. AMS 10th Conf. Atmos. Rad.*, Madison, WI, June 28 – July 2, 169-172, 1999.
18. Minnis, P. D. P. Kratz, J. A. Coakley, Jr., M. D. King, D. Garber, P. Heck, S. Mayor, D. F. Young, and R. Arduini, Cloud Optical Property Retrieval (Subsystem 4.3). In *Clouds and the Earth's Radiant Energy System (CERES) Algorithm Theoretical Basis Document, Volume III: Cloud Analyses and Radiance Inversions (Subsystem 4)*, *NASA RP 1376 Vol. 3*, edited by CERES Science Team, pp. 135-176, 1995.
19. Minnis, P., D. P. Garber, D. F. Young, R. F. Arduini, and Y. Takano, 1998: Parameterization of reflectance and effective emittance for satellite remote sensing of cloud properties. *J. Atmos. Sci.*, **55**, 3313-3339.
20. Chakrapani, V., D. R. Doelling, A. D. Rapp, and P. Minnis, 2002: Cloud thickness estimation from GOES-8 satellite data over the ARM SGP site. *Proc. 12th ARM Science Team Meeting*, April 8-12, St. Petersburg, FL, 14 pp. Available at http://www.arm.gov/docs/documents/technical/conf_0204/chakrapani-v.pdf.
21. Dong, X., P. Minnis, and B. Xi, 2004: A climatology of midlatitude continental clouds from the ARM SGP Central Facility: Part I: Low-level cloud macrophysical, microphysical and radiative properties. Submitted to *J. Climate*.
22. Smith, W. L., Jr., P. Minnis, and D. F. Young, An icing product derived from operational satellite data. *Proc. AMS 9th Conf. Aviation, Range, and Aerospace Meteorol.*, Orlando, FL, 11-15 Sept., 256-259, 2000.
23. Smith, W. L., Jr., P. Minnis, B. C. Bernstein, A. D. Rapp, and P. W. Heck, 2002: Supercooled liquid water cloud properties derived from GOES: Comparisons with in situ aircraft measurements. *10tth AMS Conf. Aviation, Range, and Aerospace Meteorol.*, Portland, OR, May 13-16, 89-92.
24. Smith, W. L., Jr., P. Minnis, B. C. Bernstein, F. McDonough, and M. M. Khaiyer, 2003: Comparison of supercooled liquid water cloud proerties derived from satelite and aircraft measurements. *Proc. FAA In-Flight Icing/De-icing International Conference*, Chicago, IL, June 16-20, CD_ROM, 2003-01-2156.
25. Minnis, P., W. L. Smith, Jr., L. Nguyen, M. M. Khaiyer, D. A. Spangenberg, P. W. Heck, R. Palikonda, B. C. Bernstein, and F. McDonough, 2004: A real-time satellite-based icing detection system. *Proc. 14th Intl. Conf. Clouds and Precipitation*, Bologna, Italy, 18-23 July.

26. Kawamoto, K., P. Minnis, W. L. Smith, Jr., and A. D. Rapp, 2002: Detecting multilayer clouds using satellite solar and IR channels. *Proc. 11th AMS Conf. Cloud Physics.*, Ogden, UT, June 3-7, CD-ROM, JP1.18.
27. Huang, J., P. Minnis, B. Lin, Y. Yi, M. M. Khaiyer, R. F. Arduini, and G. G. Mace, Advanced retrievals of multilayered cloud properties using multi-sensor and multi-spectral measurements. Submitted *J. Geophys. Res.*, 10.1029/2004JD005101, 2004.
28. Minnis, P., Y. Yi, J. Huang, and J. K. Ayers, Relationships between meteorological conditions and cloud properties determined from ARM data. Submitted *J. Geophys. Res.*, 2004